

# Sound Waves from Quenched Jets

Vladimir Khachatryan and Edward Shuryak

*Department of Physics and Astronomy, State University of New York, Stony Brook, NY 11794*  
(Dated: August 17, 2011)

Heavy ion collisions at RHIC/LHC energies are well described by the (nearly ideal) hydrodynamics. Last year this success has been extended to higher angular harmonics,  $v_n, n = 3..9$  induced by initial-state perturbations, in analogy to cosmic microwave background fluctuations. Here we use hydrodynamics to study sound propagation emitted by quenched jets. We use the so called “geometric acoustics” to follow the sound propagation, on top of the expanding fireball. The conical waves, known as “Mach cones”, turn out to be strongly distorted. We show that large radial flow makes the observed particle spectra to be determined mostly by the vicinity of their intersection with the fireball’s space-like and time-like freezeout surfaces. We further show how the waves modify the freezeout surfaces and spectra. We end up comparing our calculations to the two-particle correlation functions at RHIC, while emphasizing that studies of dijet events observed at LHC should provide much better test of our theory.

PACS numbers:

## I. INTRODUCTION

### A. Hydrodynamics and sounds

Jet-induced correlations have short and remarkable history. Two-hadron correlation functions measured in AuAu collisions at RHIC have revealed structures known as “ridge” and “shoulders” (about 2 rad away from trigger) These structures were originally believed to be associated with jets, but have recently been explained as hydrodynamical “harmonic flows”, basically a sound circles created by initial local perturbations. This subject has been discussed extensively in three papers [1–3] coauthored by one of us, which have very extensive introduction and references, to which the reader may refer. The first paper of this series [1] has been discussing some generic features of the sound propagation and possible role of electric (dual-magnetohydrodynamical) corona. The second paper [2] has included more detailed studies of the *phases* of the perturbations and possible ways of their experimental/theoretical studies. The third paper [3] used the so called *Gubser flow*, which allows analytic treatment of all angular harmonics, with and without viscosity. (One element of this last paper, the modification of the freezeout surface by the sound waves, will be extensively used at the end of this work.) While thermo/hydrodynamics was traditionally expected to work for majority of soft particles only, it describes well these harmonic flows including the so called “intermediate transverse momenta” region,  $p_t = 2 - 3 \text{ GeV}$ . Such particles are rare, about one such particle per event among thousands. So, once again, one finds that thermo/hydrodynamics is very robust and can describe not only the behavior of an average particle, but also the shape of rather far-reaching tails of thermal/hydro spectra.

These developments had (perhaps temporarily) take attention away from the issue of jets and their interac-

tion with the medium. However, as soon as the trigger hadron has  $p_t$  above the intermediate  $p_t$  domain, say  $p_t > 6 \text{ GeV}$ , it gets out of reach for collective flows and comes predominantly from hard collisions, or “jets”. So, the experimental input to the present paper are two-particle correlations in which the trigger is “hard”, while one (or more) associate particles are in the hydro domain,  $p_t = 1 - 3 \text{ GeV}$  (hard-intermediate correlations, for short).

The idea, that once the energy is deposited into the medium by a jet will be resulting in sound perturbations in the shape of the Mach cone, has been proposed in Refs [4, 5]. (It may resemble similar idea discussed in 1970’s for non-relativistic nuclear collisions. However it did not work, because nuclear matter is dilute and not a particularly good liquid, unlike sQGP under discussion now.) In the context of strongly coupled QGP, the problem has been addressed in the framework of AdS/CFT. As detailed by Chesler and Yaffe [6], and Gubser et al [7], the stress tensor solution obtained by holographic imaging is in remarkably good agreement with hydrodynamical solution detailed in [4], displaying the Mach cone in all its glory. Since the time-averaged sound velocity over the QGP, mixed and hadronic phases is  $\langle c_s \rangle \approx 0.4$ , the expected Mach cone angle

$$\theta_M = \arccos \left( \frac{\langle c_s \rangle}{v_{jet}} \right) \approx 1.159 \text{ rad} \approx 66.4^\circ \quad (1.1)$$

roughly matches the angular positions of the “shoulders” at  $\phi \approx \pi \pm \theta_M$  in the correlation functions. However, as the reader will see from what follows, a flow normal to the Mach cone is only one of several geometrical issues involved. Another, equally important effect, is the radial flow of extra matter produced by the wave. As we will see, it is defined mostly at the point where the sound cones intersect with the time-like and space-like freezeout surfaces.

One more geometrical effects come from the interplay

between the jet “stopping distance” and the actual size of the fireball (along the jet direction). Obviously, when the two are equal, the amplitude of the wave is at its maximum. This effect has been discussed before in direct hydrodynamical simulations of the cones, such as, e.g., that done by Betz et al [8], which we, to some extent, will follow.

The main technical difficulty of the problem is in correct treatment of the sound propagation on top of the expanding fireball. This problem has been first discussed by Casalderrey-Solana and Shuryak in [24] which modeled the fireball expansion by a Hubble-like overall expansion of the metric, the same Friedman-Robertson-Walker metric as used for Big Bang. (Of course, it creates new space rather than expanding, so it is not literally corresponding to the problem at hand, it was just a technical first step.) The physics focus of that paper was the effect of time-dependent sound velocity, especially if the phase transition is of the 1st order and can vanish at some interval of temperature  $T$ . The interesting finding was a creation of secondary – and convergent – sound waves. This idea was further discussed in [1] in connection with the “soft ridge” issue. However, if the current lattice data on the speed of sound are correct, the calculated effect of the reflected wave was shown to be too small to explain the “hard ridge”.

In this paper we developed a different method based on “geometric acoustics”.

Let us now explain the structure of the paper. In Sec II we work out the equations of the propagating sound in a moving fluid using the geometric acoustics [9]. We consider both relativistic and non-relativistic cases. Then in Sec III we construct the Mach cones formed by sound waves emitted by the associated jet, and circles formed by sound waves emitted by a jet which is originated at the same hard collision point but is different from the trigger and associated jets. Meanwhile, all the cones and circles are solutions of the relativistic and non-relativistic equations. In Sec IV we proceed to discussion of the issue related to intersection of the Mach cone surface with the fireball’s freezeout surface in 3D. Finally, in Sec V we calculate the spectra of secondaries comparing them with the experiment as well. We will use our assumption that most of the contribution to the spectra come from the region which is the “edge” formed by the intersection of the surfaces.

## B. Comments on the jet quenching

This complicated phenomenon, suggested by Bjorken in 1982, has very long history, which we of course would not go into here. For the purpose of this work it is not important to know the microscopic mechanism of jet quenching, and for modelling we will use simple forms of the energy  $dE/dx$  deposited into ambient matter. Thus this subsection will only include comments relevant for what follows below.

Hard collision events of partons are a particular type of “initial state perturbation”. It is important [10] that those generates *four* (not two!) jets. Two of them approximately balance their large transverse momenta. One of these two jets is the parent of hard “trigger” hadron, the other called the associate jet, propagates through the medium and deposits certain amount of energy into the ambient matter. Below we will follow what happens with it, provided it can be described hydrodynamically.

Two more bremsstrahlung cones, or jets, are directed forward and backward in the beam direction. Since these ones do not have large transverse momenta, they are rarely discussed, if at all. However, they do produce extra multiplicity, roughly the same as two other jets, which should be seen in the correlation functions. As suggested in [10], those would naturally explain the “hard ridge”, an extra structure near the trigger direction in the azimuthal angle, but long-range in the rapidity. In [1] the main puzzle has been discussed: why this perturbation remains correlated with the trigger direction rather than create a sound circle and move  $\pm 1$  radian away, creating “shoulders” instead? The suggested answer was flux tube formation, natural if hydrodynamics is elevated to dual magnetohydrodynamics. In this paper we will however not discuss that option, restraining to the usual sound waves.

For modelling energy loss one needs to know how the jet energy loss depends on the matter (entropy) density  $s(x)$  as well as the length  $L$  travelled by the jet in the matter from the moment of its production.

The simplest assumptions, resembling what happens in QED, is that it is proportional to matter density and is independent of  $x$ ,  $-dE/dx \sim s * const(x)$ . It did not however took long to notice [11, 12] that this assumption is in conflict with the experimental data, on jet quenching dependence on the azimuthal angle  $\phi$  relative to the impact parameter direction. Those usually are characterized by the parameter

$$v_2(p_t) = \langle \cos(2\phi) \rangle, \quad (1.2)$$

(not to be confused with the elliptic flow: we now hard transverse momenta  $p_t > 6 GeV$ ). This quantity can also be seen as related to the difference between the hard hadron spectra from jets travelling in the  $x$  direction ( $\phi = 0$ , in-the-reaction-plane) and in the  $y$  direction ( $\phi = 90^\circ$ , out-of-plane). Not going into the history of the  $v_2$  debate, let us comment on its current status. There are two ideas on the market, reproducing the  $v_2(p_t > 6 GeV)$  data:

- (i) One [13] is that the quenching is not proportional to density but is enhanced in the near- $T_c$  region or the so called “mixed phase”.
- (ii) Another is based on the strong coupling theory (AdS/CFT) picture of matter, resulting in the energy loss [14, 15]

$$-\frac{dE}{dx}|_{strong\ coupling} \sim T^4 x^2, \quad (1.3)$$

While this regime may look similar to the weak coupling BDMPS result

$$-\frac{dE}{dx}|_{\text{weak coupling}} \sim T^3 x \quad (1.4)$$

it is in fact qualitatively different. To see this one should recall that  $T \sim 1/x^{1/3}$  due to longitudinal expansion. As a result, the strong coupling result diverges at large  $x$ , while the weak coupling one is spread over the whole path. Thus the former one does describe the  $v_2$  data, while the latter one does not.

Two proposed explanations are very different in nature, the near- $T_c$  “blackness” of matter [13] versus physical growth of the jet “falling into the IR” in [14, 15]. Yet it is hard to tell them apart in practice, because at RHIC the near- $T_c$  region corresponds to the proper time  $\tau = 5 - 9 \text{ fm}/c$  which is very close to the typical time it takes for the associate jet to traverse the fireball. Perhaps one would need to do a detailed comparison of RHIC and LHC results to see which one describes the data better, as at LHC the near- $T_c$  region is shifted to later times.

Another feature of the strong coupling results is that large fraction of energy is released at the stopping point, see details in [16]. In our calculations below, there is one more reason for the importance of the endpoint of the jet path inside the matter: the less time perturbation in matter has to travel, the larger sound amplitude it has.

## II. SOUNDS IN A MOVING FLUID AND THE GEOMETRIC ACOUSTICS

As detailed in hydrodynamics textbooks (e.g., by Landau-Lifshitz [9]) the rays describing the sound propagation can be described in the “geometric acoustics” approximation which uses the analogy between the Hamilton-Jacobi equation for the particle and the wave sound equation. The velocity and direction of the sound propagation can be derived with the help of the eikonal function. The Hamilton equations of motion for “phonons” (or “particles” of the sound) have the following generic form

$$\frac{d\vec{r}}{dt} = \frac{\partial \omega(\vec{k}, \vec{r})}{\partial \vec{k}}, \quad (2.1)$$

$$\frac{d\vec{k}}{dt} = -\frac{\partial \omega(\vec{k}, \vec{r})}{\partial \vec{r}}, \quad (2.2)$$

driven by the (position dependent) dispersion relation  $\omega(\vec{k}, \vec{r})$ . For clarity, let us start with the simplest non-relativistic case, namely of small velocity of the flow,  $u \ll 1$ . In this case the dispersion relation is obtained from that in the fluid at rest by a Galilean transformation, so that

$$\omega(\vec{k}, \vec{r}) = c_s k + \vec{k} \vec{u}. \quad (2.3)$$

In the trivial case of the constant flow vector,  $\vec{u} = \text{const}(r)$ , the first of the above equations just obtains

an additive correction

$$\frac{d\vec{r}}{dt} = c_s \vec{n}_{\vec{k}} + \vec{u}, \quad (2.4)$$

where  $\vec{n}_{\vec{k}} = \vec{k}/k$  is the unit vector in the direction of the momentum. The second equation remains trivial

$$\frac{d\vec{k}}{dt} = 0, \quad (2.5)$$

as there is no coordinate dependence anywhere. So, a point perturbation in a moving fluid simply produces a moving sound circle. motion with the speed of sound, then the position

After this “warm-up”, let us do a non-trivial problem, simple enough to be analytically solved. Let us consider a (generalized) Hubble-like flow

$$u_i(r) = H_{ij} r_j, \quad (2.6)$$

with some time and coordinate independent Hubble tensor  $H_{ij}$ . The equation (2.2) now reads

$$\frac{dk_i}{dt} = -H_{ij} k_j. \quad (2.7)$$

So, if the Hubble tensor is symmetric and can be diagonalized with real eigenvalues  $H_1, H_2, H_3$ , then the solution in its eigenframe is exponential momentum contraction  $k_i(t) = \exp(-H_i t) k_i(0)$ . However, if the Hubble tensor contains an anti-symmetric part, the eigenvalues can be imaginary, so that the  $\vec{k}$  is rotating around the vector  $\epsilon_{ijk} H_{jk}$ .

The first equation (2.1) reads :

$$\frac{dr_i}{dt} = c_s \vec{n}_{\vec{k}}(t) + H_{ij} r_j(t). \quad (2.8)$$

In the simplest case when the Hubble matrix is proportional to the unit matrix the solution is simply a linear addition of the Hubble expansion and sound motion:

$$\vec{r}(t) = c_s t \vec{n}_{\vec{k}} + \vec{r}(0) \exp(+Ht). \quad (2.9)$$

This example can be applied to real hydro explosion, in which the late-time flow can indeed be well approximated by a Hubble form. For central collisions we will only discuss, the Hubble tensor is even isotropic. The only complications is that this pattern needs some time to be developed, so below we will use it only later than some time  $t_0 \approx 5 \text{ fm}$  [17]. So the two-dimensional form of the equations (2.1) and (2.2) to be used is

$$\begin{aligned} \frac{dk_1}{dt} &= -H k_1(t) \Theta(t - t_0) \\ \frac{dk_2}{dt} &= -H k_2(t) \Theta(t - t_0) \\ \frac{dr_1}{dt} &= c_s \cos(\theta) + H r_1(t) \Theta(t - t_0) \\ \frac{dr_2}{dt} &= c_s \sin(\theta) + H r_2(t) \Theta(t - t_0). \end{aligned} \quad (2.10)$$

The initial conditions to this system are specified as follows:

$$\begin{aligned} k_1(0) &= \cos(\theta), \quad k_2(0) = \sin(\theta), \\ r_1(0) &= x(0), \quad r_2(0) = y(0), \end{aligned} \quad (2.11)$$

where  $x(0)$  and  $y(0)$  are constants and measured by  $fm$ 's. They are the coordinates of the hard collision point where a jet is produced and simultaneously emits phonons. For the angle  $\theta$  we take the value of the Mach angle relative to the jet velocity from equation (1.1):  $\cos(\theta) \equiv \cos(\theta_M) = c_s / v_{jet}$ .

The corresponding analytical solutions will be

$$\begin{aligned} k_1(t) &= \cos(\theta) e^{-Ht\Theta(t-t_0)} \\ k_2(t) &= \sin(\theta) e^{-Ht\Theta(t-t_0)} \\ r_1(t) &= [c_s \cos(\theta) t + x(0)] \Theta(t-t_0) + \\ &\quad + \left[ \frac{c_s \cos(\theta) (1 - e^{H(t-t_0)} - 5H e^{H(t-t_0)})}{H} - \right. \\ &\quad \left. - x(0) e^{H(t-t_0)} \right] (\Theta(t-t_0) - 1) \\ r_2(t) &= [c_s \sin(\theta) t + y(0)] \Theta(t-t_0) + \\ &\quad + \left[ \frac{c_s \sin(\theta) (1 - e^{H(t-t_0)} - 5H e^{H(t-t_0)})}{H} - \right. \\ &\quad \left. - y(0) e^{H(t-t_0)} \right] (\Theta(t-t_0) - 1). \end{aligned} \quad (2.12)$$

A bunch of rays emitted to all directions from some initial point will thus be at a surface of an expanding sphere, as in constant flow:

$$(\vec{r}(t) - \vec{r}(0) \exp(+Ht))^2 = t^2 c_s^2, \quad (2.13)$$

with a sphere center moving “with a flow”.

In heavy ion collisions the explosion is relativistic, with transverse velocity reaching  $u \sim 0.7c$ . Therefore the local Galilean transformation should be substituted by the Lorentz one, which gives

$$\omega(\vec{k}, \vec{r}) = c_s k \cosh(Y) + \vec{k} \hat{u} \sinh(Y) \quad (2.14)$$

where  $\hat{u}$  means a unit vector in the direction of  $u$ , and  $Y$  is the rapidity. Now it is no longer possible to separate the equations (2.1) and (2.2), and they should be solved together numerically. Substitution of the equation (2.14) into (2.1) and (2.2) gives us the following system of four differential (relativistic) equations:

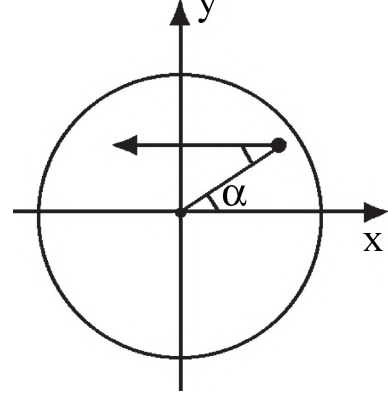


FIG. 1: The  $\alpha$  is the angle between the associated jet's momentum and the axis  $x$ . The arrow inside the circle is the momentum of the associated jet which originates from the hard collision point opposite to the trigger jet (not shown) in the  $x$  direction.

$$\begin{aligned} \frac{dk_1}{dt} &= -c_s \sqrt{k_1^2 + k_2^2} \times \\ &\quad \times \frac{\partial}{\partial r_1} \left( \frac{1}{\sqrt{1 - H^2(r_1^2 + r_2^2)\Theta(t-t_0)}} \right) - \\ &\quad - k_1 \frac{\partial}{\partial r_1} \left( \frac{H r_1 \Theta(t-t_0)}{\sqrt{1 - H^2(r_1^2 + r_2^2)\Theta(t-t_0)}} \right) - \\ &\quad - k_2 \frac{\partial}{\partial r_1} \left( \frac{H r_2 \Theta(t-t_0)}{\sqrt{1 - H^2(r_1^2 + r_2^2)\Theta(t-t_0)}} \right) \\ \frac{dk_2}{dt} &= -c_s \sqrt{k_1^2 + k_2^2} \times \\ &\quad \times \frac{\partial}{\partial r_2} \left( \frac{1}{\sqrt{1 - H^2(r_1^2 + r_2^2)\Theta(t-t_0)}} \right) - \\ &\quad - k_1 \frac{\partial}{\partial r_2} \left( \frac{H r_1 \Theta(t-t_0)}{\sqrt{1 - H^2(r_1^2 + r_2^2)\Theta(t-t_0)}} \right) - \\ &\quad - k_2 \frac{\partial}{\partial r_2} \left( \frac{H r_2 \Theta(t-t_0)}{\sqrt{1 - H^2(r_1^2 + r_2^2)\Theta(t-t_0)}} \right) \\ \frac{dr_1}{dt} &= c_s \frac{k_1}{\sqrt{k_1^2 + k_2^2}} \frac{1}{\sqrt{1 - H^2(r_1^2 + r_2^2)\Theta(t-t_0)}} + \\ &\quad + \frac{H r_1 \Theta(t-t_0)}{\sqrt{1 - H^2(r_1^2 + r_2^2)\Theta(t-t_0)}} \\ \frac{dr_2}{dt} &= c_s \frac{k_2}{\sqrt{k_1^2 + k_2^2}} \frac{1}{\sqrt{1 - H^2(r_1^2 + r_2^2)\Theta(t-t_0)}} + \\ &\quad + \frac{H r_2 \Theta(t-t_0)}{\sqrt{1 - H^2(r_1^2 + r_2^2)\Theta(t-t_0)}}, \end{aligned} \quad (2.15)$$

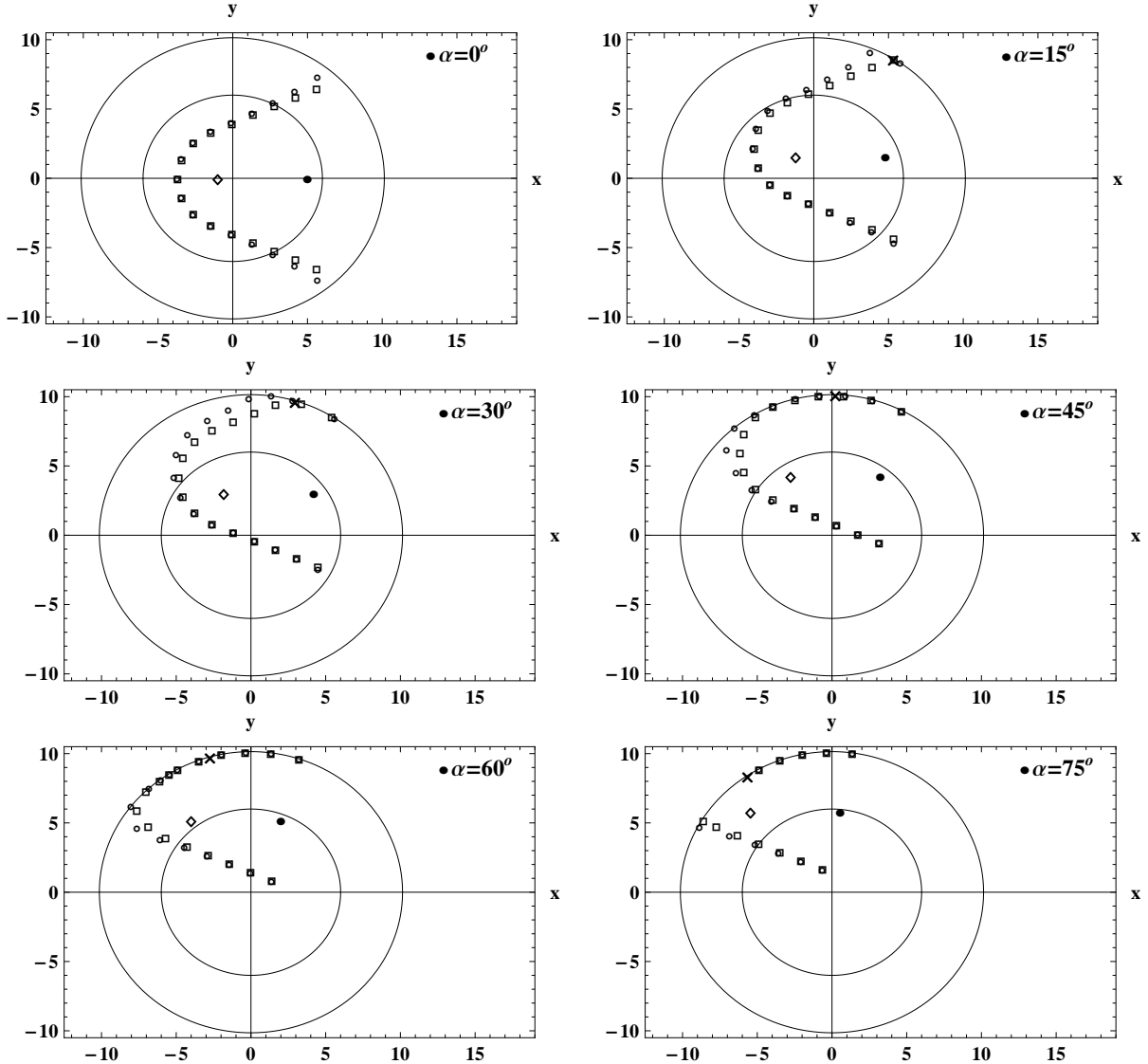


FIG. 2: (Color online) A Mach cone originated from a jet moving to the left from the point  $x(0) = 5.0 fm$  and  $y(0) = 0 fm$  at the angle  $\alpha = 0$ . The path of the jet corresponds to  $L_{stopping} = 6 fm$ , the radius of the inner circle -  $R_{in} = 6 fm$ , and the radius of the outer circle, containing the fireball at its highest extension  $R_f = \exp(H \cdot (t_f - t_0)) \simeq 10.14 fm$ . The cone created by the open squares is the solution of the non-relativistic equations (2.10), and the cone created by the open circles is the solution of the relativistic equations (2.15). The filled circle shows the hard collision point, and the open diamond shows the stopping point of the jet. The values of the angle  $\alpha$  shown in each figure, is defined in Fig.1.

with the same initial conditions as in (2.11).

### III. DISTORTED CONES AND CIRCLES OF THE EXPANDING FIREBALL

We solve the systems of equations (2.10) and (2.15) at freezeout time  $t_f = 12 fm$ , speed of sound  $c_s = 0.4$ , and the Hubble constant  $H = 0.075 fm^{-1}$ . The  $t_f$  is the time at which the fireball reaches the freeze-out temperature. (In Appendix A, we clarify a value for the freezeout time used, along with establishing the kinetic freezeout temperature.)

In order to simplify geometry of the collision, we consider only central  $Au - Au$  collisions. The notations are explained in Fig. 1: jets which have different impact parameters in respect to the fireball are defined via the angle  $\alpha$ , between the direction of the associate jets' momentum and the axis  $x$  in which the trigger jets go. (We do not show the trigger jet in Fig. 1) as a reminder that we do not include the sounds from it in what follows,

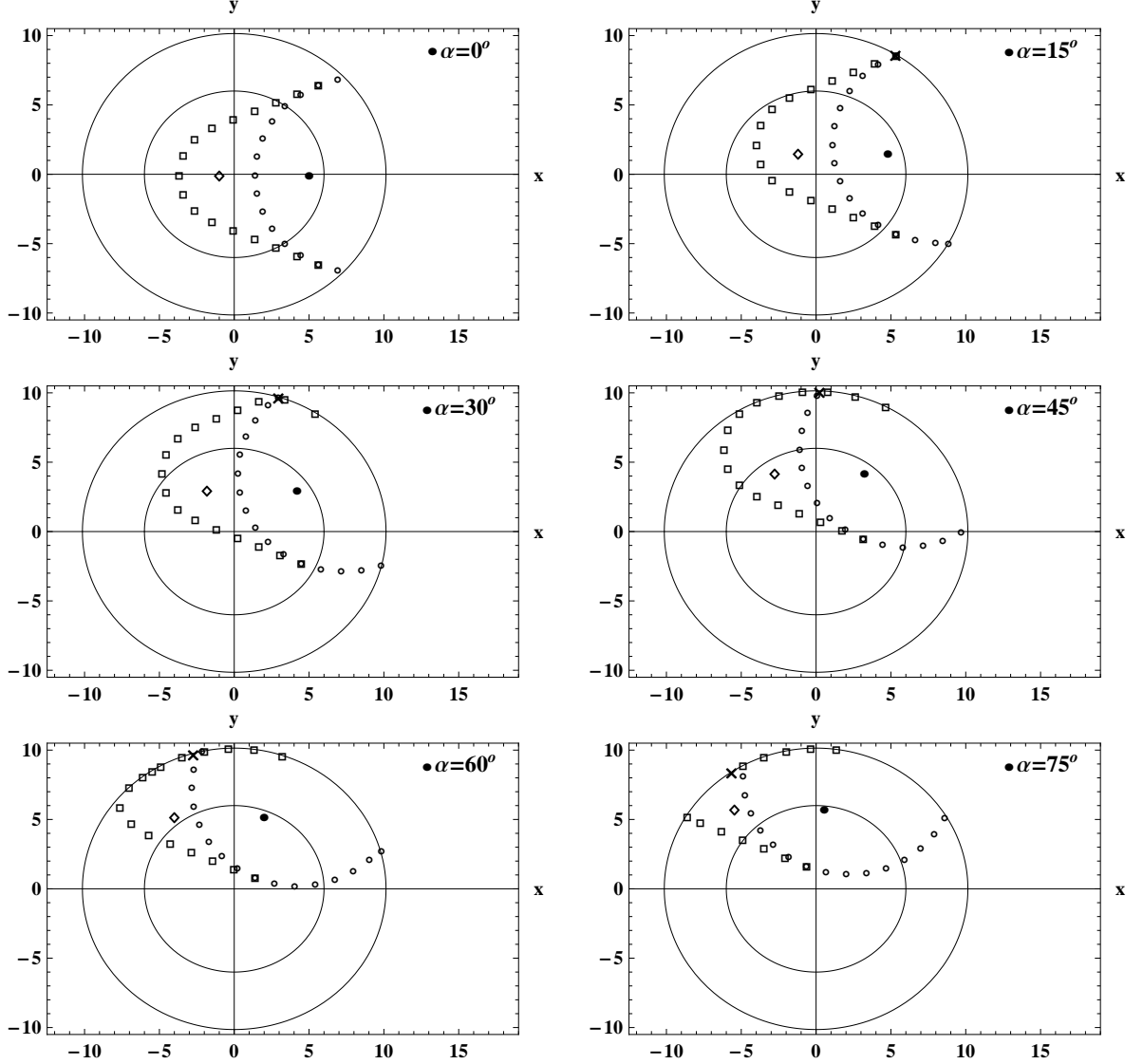


FIG. 3: The Mach cone (open squares) as in Fig. 2, and the ring (open circles) which is originated from the hard collision point  $x(0) = 5.0 \text{ fm}$  and  $y(0) = 0 \text{ fm}$  at the angle  $\alpha = 0$ . These two structures are the solutions of the non-relativistic equations (2.10).

considering its energy loss to be negligible. Due to trigger bias effect, we place hard scattering events at fixed distance, 1 fm, from the nuclear edge.)

Quenching of the associate jet is the source of the phonons, emitted from its path along the Mach direction. After that they move along the phonon rays as detailed in the previous section. We show only solutions in the upper part of the transverse plane of the fireball, binning angle  $\alpha$  into six bins  $\alpha = 0, 15^\circ, 30^\circ, 45^\circ, 60^\circ$  and  $75^\circ$ , which are depicted in Fig. 2. The case of  $\alpha = 90^\circ$  does not give rise to any conical structure since the jet at this point only strikes the edge of the fireball/inner sphere leaving it totally, without making phonons propagate in the medium. The solutions in the lower part are symmetrical to those in the upper part, that's why

they are not shown. The conical and ring structures are the solutions of the systems of equations: non-relativistic (2.10) and relativistic (2.15).

Note that in all these six figures the jets move to the left with the speed of light, from points of their production, located inside the inner circle at a distance 1 fm from that circle which in fact is the surface of a nucleus. This inner circle corresponds to the case of  $t_f = 0 \text{ fm}$ , when the fireball/inner sphere initially is not expanded as a whole. The outer circle corresponds to the radius  $t_f = 12 \text{ fm}$ , it shows the maximal extension of the fireball reached by this time.

The jet quenching discussed in those figures assume the stopping distance of the jets be  $L_{\text{stopping}} = 6 \text{ fm}$ , shown by the diamonds. ( For comparison purposes

we have also calculated cones for the stopping distance  $L_{\text{stopping}} = 12 fm$  not shown, with similar results to those in Figs. 2 except for different “rounding” of it does not matter much.) This means that we assume the jet energy and the energy loss are related by  $E/|dE/dx| = 6 fm$ . The actual values of  $E, dE/dx$  are not important for these plots and will matter only later, when we will determine the actual spectra modification.

We see that at the angles increasing towards higher  $\alpha$ , the conical structure created by the phonons has a distorted/crooked shape, which is due to the Hubble expansion starting from  $t_0 \approx 5 fm$ . The jets, produced at low and intermediate angles, do not reach the edge of the outer sphere, meaning that they do not leave the fireball. However, at the higher angles, some jets go out from the fireball at some values of the time within the range of  $t_f = 5 - 12 fm$ . One conclusion is that in the fireball with the given kinematical and dynamical conditions, the shapes of the Mach cones do not differ from each other significantly obtained from the non-relativistic equations (2.10), and from relativistic equations (2.15). Therefore, hereinafter we can consider only one of these cases, namely one can take the non-relativistic case for carrying out the other calculations.

We already mentioned above two more jets which are also created by a hard collision which move perpendicularly to the transverse plane along the beam directions. These two longitudinal jets are approximately rapidity-independent source which also may emit the sound waves. Their propagation we calculated using the same equations (2.10) but with the initial conditions in (2.11), where  $\theta$  ranges from 0 to  $360^\circ$ . Such (rapidity-independent) sound circles are depicted in Figs. 3 together with the cones (which are for one rapidity only, namely that of the associate jet). We will not use those circles below: in fact we have calculated them in order to compare to what is calculated in [3] by a different method.

#### IV. INTERSECTION OF THE MACH SURFACE WITH TIMELIKE AND SPACELIKE FREEZEOUT SURFACES

Standard expression for a particle spectrum, known as Cooper-Frye formula [31], is a thermal spectrum boosted by the 4-vector of the flow velocity  $u^\mu$  and integrated over the 3 – dimensional freezeout surface.

$$E \frac{dN}{d^3p} = \int_{\sigma_t + \sigma_s} d\Sigma_\mu p^\mu f\left(\frac{p^\nu u_\nu}{T}\right), \quad (4.1)$$

where  $\sigma_t$  and  $\sigma_s$  are time-like and space-like parts of the freezeout surface, respectively. The function  $f$  is Bose/Fermi/Boltzmann distribution, for pions it is

$$f\left(\frac{p^\nu u_\nu}{T}\right) = \frac{1}{\exp(-p^\nu u_\nu/T) \pm 1} \quad (4.2)$$

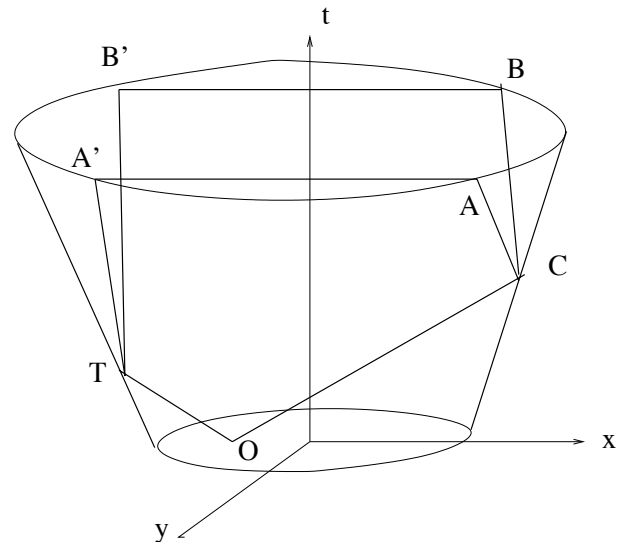


FIG. 4: The schematic shape of the Mach surface in the transverse  $(x, y)$  plane at  $z = 0$  and fixed time (upper plot), as well as its shape in 3d including the proper longitudinal time (lower plot). The Mach surface  $\sigma_M$  is made of two parts,  $OCAA'T$  and  $OCBB'T$ . This figure is from [30].

simply corresponds to the thermal distribution of matter inside the fluid cells. (If needed, the function can be appended by an anisotropic part corresponding to viscosity.)

We will be interested in a special case of this distribution in the region where, at one hand, the hydrodynamics works well, and on the other, the ratio  $(p_t/T_f)$  is as large as possible. (As we are only interested in the tail of the function  $f$ , so that the Boltzmann approximation will always be enough.) This ratio, if large, strongly enhances the effect of the small perturbation, the sounds, on the particle spectrum. In fact, for  $p_t = 1 GeV$  and  $p_t = 2 GeV$  we will be using below, this large ratio time small amplitudes of the sound waves is able to produce effects of the order  $O(1)$  in the exponent. This interplay of large  $p_t/T_f$  and small sound wave is one of the core ideas of this paper.

Before we go to details about realistic freezeout surfaces, in the next section and Appendix A, we would like to introduce another qualitative idea, this time related with the radial flow. The concept has been introduced in [30] and is explained in schematic way in Fig. 4. (Note that in Fig. 4 it is assumed that the associated jet propagates to the right, unlike in the conventions above.) It shows the picture in 3d, at fixed longitudinal coordinate  $z = 0$ . The proper time  $\tau$  runs upward, and the upper circle schematically represents the time-like part of the freezeout surface,  $\sigma_t$ , approximated by the constant time surface,  $t = t_f$ . The lower circle is the so called “initiation time surface”, and the conical surface connecting the two ellipses is our approximation to the space-like part of the freezeout surface,  $\sigma_s$ . The points  $A, B, A'$  and

$B'$  are the intersection of the sound waves with  $\sigma_t$ , and the region between them contains matter affected by the waves: outside it is not affected, by hydro causality. The points  $T, C$  are intersections of the trigger and the companion jets with  $\sigma_s$ . The main idea is that the vicinity of four points  $A, B, A'$  and  $B'$  should dominate the spectra (modified by the sounds) because the large upper circle is where the radial flow is at its maximum. (We will return to this idea at the quantitative level in the next section.)

Let us now promote this figure from 3-dimension to all 4, by adding the longitudinal  $z$  direction. We cannot plot it in full, and therefore limit ourselves to the  $t = t_f$  time slice. Since we have the intercept of 3 surfaces ( $\text{Mach}, \sigma_t, \sigma_s$ ) in 4d, it must be a 1-dimensional curve. It is in fact two ellipses, one having points  $A, B$  on it, and the other having  $A', B'$ . Let us call these two edges  $\epsilon_C$  and  $\epsilon_T$ , for the companion (associated) jet and the trigger jet, respectively. (Since the trigger-bias forces the associated jet to deposit much larger amount of energy, the former one has much larger chance to become visible.)

Let us calculate the extension of these elliptic curves into the longitudinal coordinate  $z$  direction, or rather its proxy, the pseudo-rapidity  $\eta$ . In Figs. 5, 6, 7 and 8 we show correspondingly the edges  $\epsilon_C$  (ellipses) created by phonons at  $t_f = 12 fm$ , emitted by a jet whose momentum is directed as in Figs. 2. However, now the increase of the angle  $\alpha$  from the previous jet to the next one is  $\Delta\alpha = 5^\circ$ , rather than  $15^\circ$ . Again the case of the jet produced at  $\alpha = 90^\circ$  is ignored. Besides, we also consider phonons (from all the jets under consideration) moving in the lower hemisphere of the fireball. The total number of all the considered jets (events) is thirty.

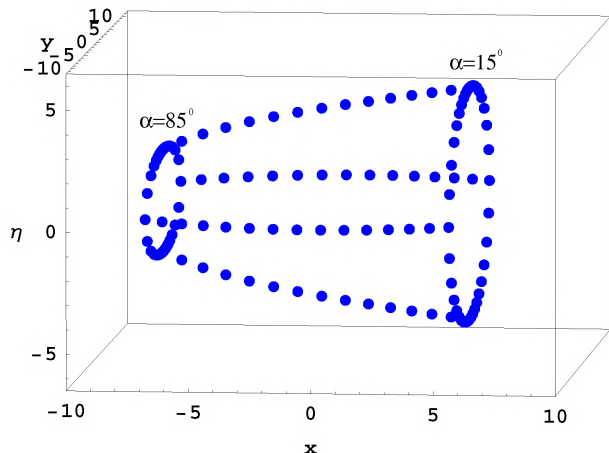


FIG. 5: (Color online) Two elliptic structures correspond to the edges  $\epsilon_C$  produced by phonons at intersection of all the three surfaces. These phonons in turn are emitted by an associated jet which moves in the  $x$  direction (or parallel to it) emitting the phonons in  $x, y$  and  $\eta$  directions. The largest ellipse corresponds to the jet with  $\alpha = 15^\circ$ , and the smallest ellipse corresponds to the jet with  $\alpha = 85^\circ$ .

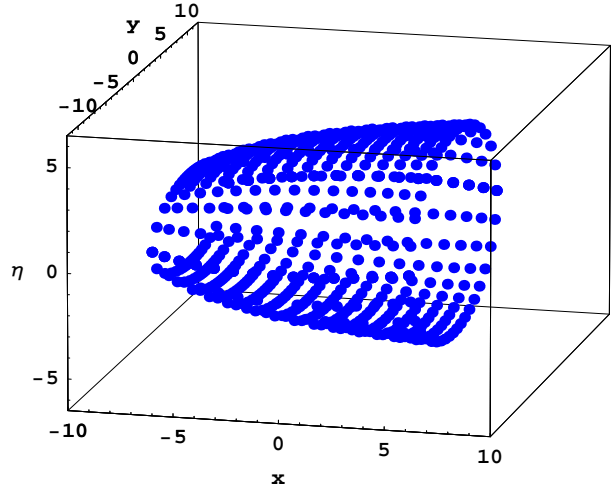


FIG. 6: (Color online) The same figure as in Fig. 5 but which is complete including the contributions of all the jets with  $\alpha = 15^\circ \div 85^\circ$ .

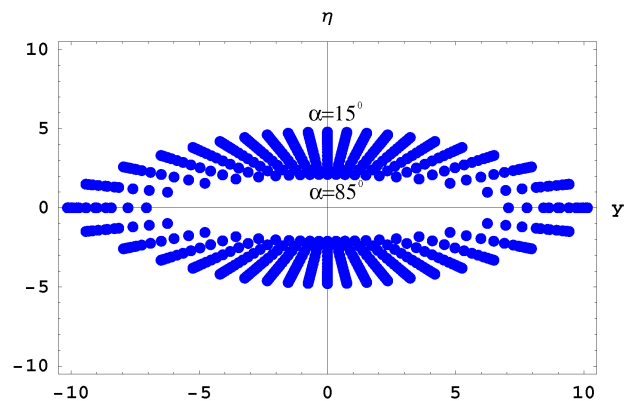


FIG. 7: (Color online) The same figure as in Fig. 6 but in the  $(\eta, y)$  plane. The largest ellipse corresponds to the jet with  $\alpha = 15^\circ$ , and the smallest ellipse corresponds to the jet with  $\alpha = 85^\circ$ .

## V. APPLICATION TO PARTICLE SPECTRA WITH THE MODIFIED FREEZEOUT SURFACE

The temperature and velocity in Cooper-Fry formula have complicated space-time dependence derived from hydrodynamics. As in [3] we assume that the freezeout surface is an isotherm of the form of  $T(t, r) = T_f$ . Accordingly, the time-like part of the surface, for example, can be written as

$$\Sigma^\mu = (t_f(x, y), x, y, \eta). \quad (5.1)$$

So at the time  $t_f(x, y)$  the fireball reaches the freezeout temperature  $T_f$ . Note that (4.1) contains the vector normal to the surface. As to the element of the surface, it is



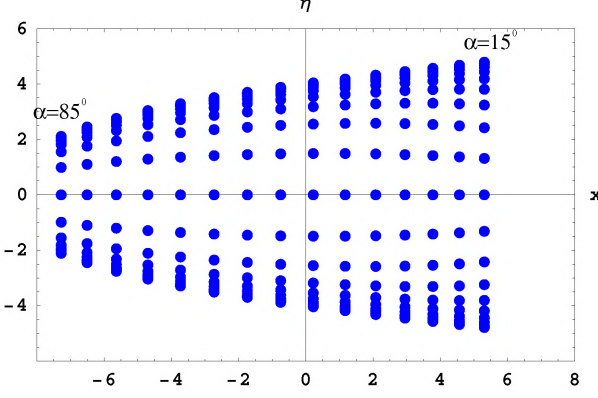


FIG. 8: (Color online) The same figure as in Fig. 6 but in the  $(\eta, x)$  plane. The largest vertical corresponds to the jet with  $\alpha = 15^\circ$ , and the smallest vertical corresponds to the jet with  $\alpha = 85^\circ$ .

represented as

$$\begin{aligned} d\Sigma_\mu &= \sqrt{-g} \epsilon_{\mu\nu\lambda\rho} \frac{\partial \Sigma^\nu}{\partial x} \frac{\partial \Sigma^\lambda}{\partial y} \frac{\partial \Sigma^\rho}{\partial \eta} dx dy d\eta = \\ &= \left( -1, \frac{\partial t_f}{\partial x}, \frac{\partial t_f}{\partial y}, 0 \right) t_f dx dy d\eta \\ &= -t_f dx dy d\eta + t_f dt_f dy d\eta + t_f dt_f dx d\eta, \end{aligned} \quad (5.2)$$

where  $g$  is the determinant of the metric and  $\epsilon_{\mu\nu\lambda\rho}$  is the Levi-Civita symbol.

For  $p_\mu d\Sigma_\mu$  and  $p_\mu u^\mu$  one may use the formulae from Ref. [32] which are the following:

$$\begin{aligned} p_\mu d\Sigma^\mu &= \left( m_t \cosh(\eta - y) - \right. \\ &\quad \left. - p_t \cos(\phi - \phi_p) \frac{dt_f(r)}{dr} \right) t_f(r) r dr d\phi d\eta, \end{aligned} \quad (5.3)$$

$$p_\mu u^\mu = (m_t \cosh(\eta - y) u^\tau - p_t \cos(\phi - \phi_p) u^r) \quad (5.4)$$

where  $u^\tau = \gamma = (1 - u(r)^2)^{-1/2}$ ,  $u^r = u(r)u^\tau$  (with  $u(r)$  given by (2.6)),  $m_t = \sqrt{p_t^2 + m_\pi^2}$  (the  $m_\pi$  is the pion mass). We extract the function  $t_f(r)$  from hydro solutions discussed in Appendix A.

For each  $p_t$  and the direction of the particle  $\phi_p$  there is a point on the freezeout surface which maximally contribute to the spectrum. Indeed, the radial flow grows with  $r$  and enhance the spectrum, but the surface itself makes a turn and ends. One can determine the spectrum from the Cooper-Fry formula and compare it to e.g. Gaussian approximation around this point. Those two are shown in Fig. 9, as a particular example. The lesson is that there exist a sharp peak near the fireball's edge, at which the quest for the strongest radial flow and for the largest amount of surface area (and thus multiplicity) are in the best compromise. We have checked

that those peaks indeed produce the spectra in agreement with what hydro papers reported, and with what are observed experimentally. This confirms that the tails of the spectra we are interested are dominated by the vicinity of such points.

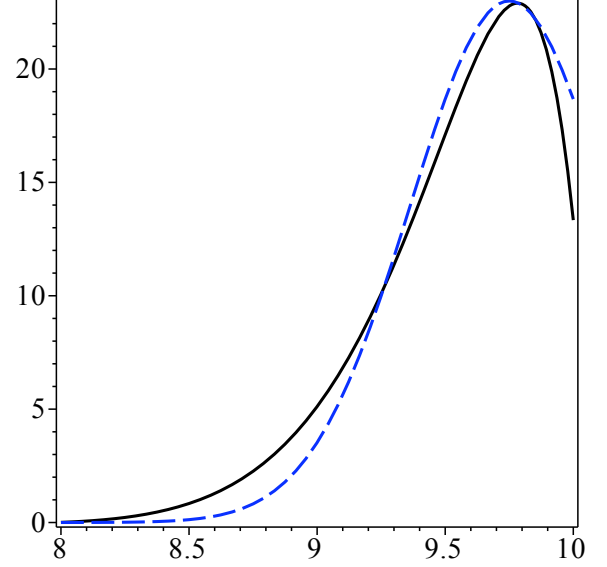


FIG. 9: (Color online) The contribution to the pion spectrum (arbitrary units) vs the radial coordinate  $r$  (fm). The solid (black) curve is the Cooper-Fry formula for  $p_t = 2 \text{ GeV}$ ,  $T_f = .12 \text{ GeV}$ , the dash (blue) curve is the Gaussian approximation mentioned in the text.

Now we consider the effect of sound perturbations on the particles (pions) spectra. Here we follow the discussion of [3] since the same process occurs in our case. The perturbations can affect the spectra in two ways. We have two variables which have their contributions: namely, the flow velocity  $u_\mu$  and temperature  $T$ . The first effect is related to the  $u_\mu$  in the exponent of (??) which should be corrected by an extra term of the first order due to sound. The second effect is related to the first order  $T$  perturbations. One can consider the so called “zeroth” order fireball and the fireball with the “hot spot” induced by an initial-state perturbation. In the presence of this “hot spot” the corresponding perturbation in temperature,  $\delta T$ , is positive and implies a production of extra particles as compared to the zeroth order fireball. The  $\delta T$  locally delays the freezeout temperature by the formula

$$T_0(t, r) + \delta T(t, r) = T_f, \quad (5.5)$$

which also provides an extra volume for containing the produced extra particles. Thus the freezeout surface is deformed in terms of the temperature and volume. Generally, it provides a little larger flow as compared to that of the zeroth order fireball.

The velocity perturbation,  $\delta u_\mu$ , added to the velocity  $u_\mu$  gives

$$u_\mu \rightarrow u_\mu + \delta u_\mu. \quad (5.6)$$

In order to find  $\delta T$  and  $\delta u$  we make use of well known hydrodynamical relations:

$$n = \frac{g'}{\pi^2 \hbar^3} T^3, \quad (5.7)$$

$$\epsilon = 3p = 3nT. \quad (5.8)$$

The  $g'$  is the total degeneracy factor which counts the total number of degrees of freedom, summed over the spins, flavors, charge (particle-antiparticle) and colors of particles. For the QGP,  $g' \approx 3$  at freezeout. From the equations (5.7) and (5.8) one obtains

$$\delta T = \left( \frac{\pi^2 \hbar^3}{12g'} \right) \frac{\delta \epsilon}{T^3}. \quad (5.9)$$

In the denominator we can take  $T^3 \approx T_f^3$ .

The next step is to use the first order velocity perturbation from Ref. [9] which is of the form of

$$\delta u = -c_s \frac{\delta \epsilon}{(\epsilon_0 + p_0)}. \quad (5.10)$$

With the corresponding substitutions from (5.7), (5.8) and (5.9), the equation (5.10) results in

$$\begin{aligned} \delta \vec{u}^{(1)} &= -3c_s \frac{T^3}{T_0^4} \delta T \vec{n}_{\vec{k}} \approx \\ &\approx -3c_s \frac{\delta T}{T_f} \vec{n}_{\vec{k}}, \end{aligned} \quad (5.11)$$

where  $\vec{n}_{\vec{k}}$  is the unit vector in the direction of the momentum of phonons which are located in the points of the “crosses” in the transverse  $xy$  plane, such as in Fig.2. Thus we have the equations (5.9) and (5.11) which determine the first order perturbations of the temperature and velocity. The only unknown is the perturbation in energy density,  $\delta \epsilon$ , which should be found as well. In the appendix we work out the procedure by which the  $\delta \epsilon$  is determined from the wave equation (see Appendix B for more details).

However, there is also another effect related to the  $\delta u$  which is of the first order of perturbation due to expansion of the fireball:  $\delta u = H \delta r$ , where  $r$  is the radial distance from the center of the fireball. From our hydro parameterizations we have found an approximate function for the temperature (at freezeout time  $t_f = 12 fm$ ) as a function of  $r$ . It is approximated as

$$T(t_f, r) \approx \left( \frac{-1.75 r^2}{fm^2} + \frac{19.20 r}{fm} + 99.67 \right) MeV. \quad (5.12)$$

It is relevant to note that the  $\delta r$  gives the increase of the fireball's volume (also giving rise to  $\delta T$ ). It is equal to

$$\delta r = \frac{\delta T(t, r)}{[\partial T(t_f, r)/\partial r]|_{r_f}}. \quad (5.13)$$

The  $\delta T$  is determined from (5.9) which, e.g., for  $dE/dx = 1 GeV$  turns out to be  $4 \div 5 MeV$  depending on the angle  $\phi$ . Then due to the effect of the volume change we will have

$$\begin{aligned} \delta \vec{u}^{(2)} &= H \delta r \vec{n}_{\vec{r}} = \\ &= H \frac{\delta T(t, r)}{[\partial T(t_f, r)/\partial r]|_{r_f}} \vec{n}_{\vec{r}}, \end{aligned} \quad (5.14)$$

where  $\vec{n}_{\vec{r}}$  is the unit vector in the radial direction of the phonons at the points of the “crosses” in the transverse  $xy$  plane, such as in Fig.2. Thus taking into account all the above-mentioned effects, for the exponent in the Cooper-Frye formula one can write

$$\frac{p^\mu u_\mu}{T_f} = \frac{p_0 u_0}{T_f} + \frac{\vec{p} \vec{u}}{T_f}. \quad (5.15)$$

With the perturbations one obtains

$$\frac{\vec{p} \vec{u}}{T_f} \rightarrow \frac{\vec{p} \vec{u}}{T_f} + \frac{\vec{p} \delta \vec{u}^{(1)}}{T_f} + \frac{\vec{p} \delta \vec{u}^{(2)}}{T_f}, \quad (5.16)$$

where  $|\delta \vec{u}^{(1)}| = \delta u^{(1)}$  determined from (5.11), and  $|\delta \vec{u}^{(2)}| = \delta u^{(2)}$  determined from (5.14).

In heavy ion collisions some amount of secondaries originate from jets produced via hard scattering. When the transverse momentum  $p_t$  is large enough, the hard component of it (in the spectrum of particles) “suppresses” the hydrodynamical spectrum, though the jet quenching can be significant. So the hydrodynamics does not work at large  $p_t$ 's. Such a case occurs also at relatively large viscous corrections to the viscous term in the stress tensor. These corrections get larger with increase of  $p_t$ , and will not be small at some point when one compares them with the ideal term of the stress tensor.

## VI. COMPARISON TO THE RHIC DATA

Finally, we can carry out calculations of the pions' spectra including the sound wave perturbations, and do a comparison with the STAR's two-pion correlation functions.

The effect of both components of the flow we called above  $\delta u^{(1)}, \delta u^{(2)}$  are calculated, for each  $\alpha$ , and then summed over. We remind that the former effect is the effect of perturbed flow, normal to Mach cone, and the latter is the effect of extra matter added by the wave, which flows together with the rest of matter in the local radial flow direction. The results, for  $p_t = 1$  and  $2 GeV/c$  are shown in Fig. 10. As shown there, the average over half plane produce a signal shifted in angle,

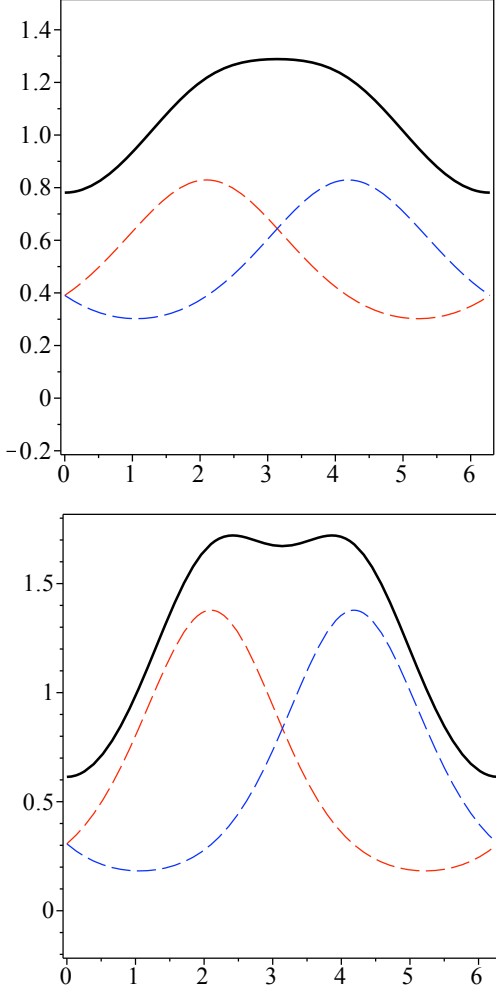


FIG. 10: (Color online) The spectrum vs  $\phi_p$  at  $p_t = 1 \text{ GeV}$  and  $2 \text{ GeV}$ , for  $dE/dx = 1 \text{ GeV}/fm$ . The contribution to the spectrum mostly comes from a phonon at the “cross” in Fig.2. The red and blue dashed lines show contributions of the jets in the upper ( $\alpha > 0$ ) and lower ( $\alpha < 0$ ) half plane in Fig.1.

but in average together with another half-plane it creates a plateau-like sum. As  $p_t$  grows, it starts develop a double-hump structure reminiscent of the original Mach cone predictions (but with a different angle).

An example of hard-soft correlation function exhibited in Fig. 11 is from STAR publication [33]. The trigger  $p_t = 6..10 \text{ GeV}$ , which we consider to be well in the hard hadron domain. The open (black) circles correspond to dAu collision and are shown for comparison only, as in this case there is no matter for jets to interact with: they display narrow peak at  $\phi = \pi$ . The central AuAu data are shown by (blue) filled circles and open (red) squares, for two rapidity slices. Two pictures are for two bins of the associate particle (see the captions).

The overall shape and the width of the angular distri-

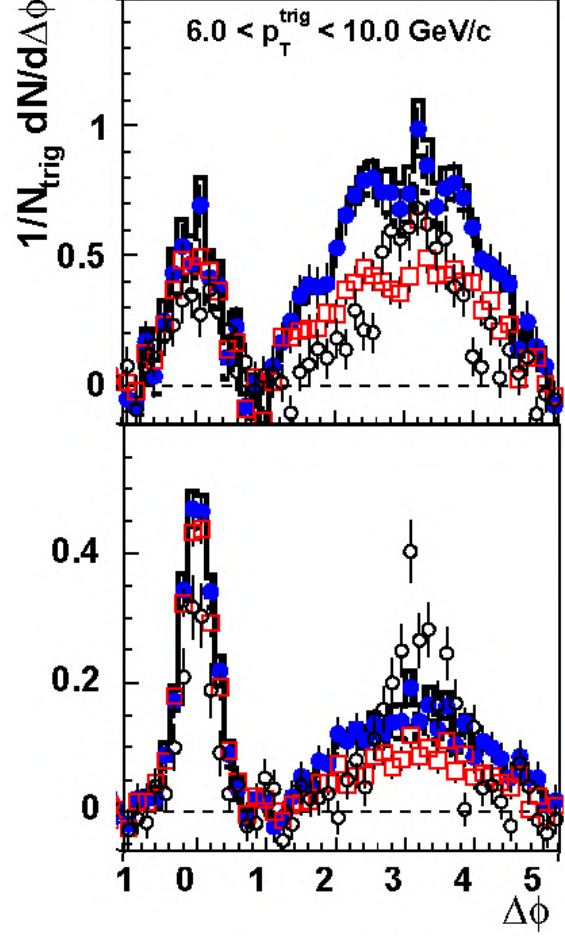


FIG. 11: (Color online) From [33]. Background-subtracted azimuthal angle difference distributions for near-central collisions (fraction of the total cross section 0-12%). The associated particles have the range of  $p_T$  between  $0.5 - 1 \text{ GeV}/c$  (upper figure), between  $1.5 - 2.5 \text{ GeV}/c$  (lower figure), and the trigger particles have  $p_T$  ranging from  $6.0$  to  $10.0 \text{ GeV}/c$ . The data for Au+Au collisions are shown by the solid circles and for d+Au by the open circles. The rapidity range is  $|\eta| < 1$  and as a result the rapidity difference is  $|\Delta\eta| < 2$ . Open red squares show results for a restricted acceptance of  $|\Delta\eta| < 0.7$ . The solid and dashed histograms show the upper and lower range of the systematic uncertainty due to the  $v_2$  modulation subtracted.

bution seem to be reproduced by the theory.

While comparing the two, one should however remember that:

- (i) our calculation include only energy deposited into the media and the sound waves. Sufficiently peripheral jets (with  $\alpha \approx 90^\circ$ ) have punch-through remnants of the jets which are not included. This component is increasing with associate particle  $p_t$ , filling the place between the two humps in the lower picture.
- (ii) theory calculation is done for pions having the same

rapidity as the associate jet, while the data are for certain rapidity interval. However, as comparison of the solid (blue) circles and open (red) squares shows, the difference in shape is not too strong. This issue definitely need to be studied more, to separate what we call “cone” from the rapidity-independent “circles”.

(iii) theory calculation have no fluctuations in  $dE/dx$ , and thus assume completely deterministic scenario in which all jets stop at some fixed points, when its energy is all lost. Perhaps in reality fluctuations are not small, and there are punch-through jets at any  $\alpha$ .

Completing the paper we emphasize that new data from LHC have well reconstructed di-jet events, in which transverse momenta and rapidities of both trigger and associate jets are detected. Soft particles angular distributions, both in azimuth and rapidity, will obviously provide much better understanding of the issues involved. However current statistics of such events  $\sim 1000$  is perhaps too small to address it. We will report calculations of the sound wave contributions in such conditions elsewhere.

**Acknowledgments.** This work was supported in parts by the US-DOE grant DE-FG-88ER40388.

## VII. APPENDIX A: THE FREEZEOUT SURFACE

We approximate the freezeout surface as the isotherm, with  $T_f = 120 \text{ MeV}$ . The parameterization of it is based on the results of other authors, namely Refs. [17], [25] and [26]. The surface we use is parameterized as

$$\begin{aligned} \tau(r) = & -0.0011 * r^5.995 + 0.0266 * r^4.99762 \quad (7.1) \\ & -0.2367 * r^4 + 0.9772 * r^3 - 1.9095 * r^2 \\ & + 0.7 * r + 17.657 \end{aligned}$$

In [17], it was noted that the freezeout time changes only a little if one goes from SPS ( $t_f = 10 \text{ fm}$ ) to RHIC ( $t_f = 11 \text{ fm}$ ). In [25], the freezeout time for central collisions is calculated to be  $\approx 12 \text{ fm}$  (at  $T_f = 130 \text{ fm}$  for RHIC) In [26], the value obtained for the freezeout time is  $t_f = 12 \text{ fm}/c$ , however, the temperature distributions can have sizable spreads in the range of  $\sim 100 - 160 \text{ MeV}$ . In [27], having the results of [28], it was pointed out that the evolution time to kinetic freezeout - say until  $T_f \approx 140 \text{ MeV}$  is  $t_f \sim 12 - 14 \text{ fm}/c$  in both cases of longitudinal and transverse dynamics; the timescale which is most directly probed by femtoscopy. Nonetheless, from all these scenarios, having a worked out combined scenario from [17] and [25] at our disposal, we take the aforementioned values for the freezeout time and “kinetic” temperature as averaged values for our ansatz: namely  $< t_f > \equiv t_f = 12 \text{ fm}$  and  $< T_f > \equiv T_f = 120 \text{ fm}$ . Such a combined scenario is based on the joint consideration of these papers.

Usually one separates “kinetic” and “chemical” freezeouts in which elastic and inelastic scattering rates are involved. Since different secondaries (pions,  $K$  mesons, nucleons,  $J/\psi$  particles, etc) in fact have quite different elastic cross sections, the “kinetic” surfaces should be different for each species. We do not discuss all such complications in our work, and consider only one type of secondaries, the pions, the spectra of which are shown in the last section.

## VIII. APPENDIX B. NORMALIZATION OF THE MACH CONE WAVE

Suppose that the relative changes of the density  $\rho$  and pressure  $p$  in the medium of the fireball are much small as compared to their unperturbed values:  $\delta p \ll p_0$  and  $\delta \rho \ll \rho_0$  such that

$$p = p_0 + \delta p \quad \text{and} \quad \rho = \rho_0 + \delta \rho. \quad (8.1)$$

Suppose that this is also the case for the velocity of particles of the medium:  $u \ll c_s$ .

Then having the continuity equation and Euler’s equation

$$\begin{aligned} \frac{\partial \rho}{\partial t} + \vec{\nabla} \cdot \rho \vec{u} &= 0 \\ \frac{\partial \vec{u}}{\partial t} + (\vec{u} \cdot \vec{\nabla}) \vec{u} &= -\frac{\vec{\nabla} p}{\rho}, \end{aligned} \quad (8.2)$$

one can rewrite this system as

$$\begin{aligned} \frac{\partial(\delta \rho)}{\partial t} + \rho_0 \vec{\nabla} \cdot \vec{u} &= 0 \\ \frac{\partial \vec{u}}{\partial t} + \frac{\vec{\nabla}(\delta p)}{\rho_0} &= 0. \end{aligned} \quad (8.3)$$

If now we proceed to relativistic notations  $\delta \rho = \delta \epsilon$  and  $\rho_0 = \epsilon_0 + p_0$ , then the system (8.3) will have the following form:

$$\begin{aligned} \frac{\partial(\delta \epsilon)}{\partial t} + (\epsilon_0 + p_0) \vec{\nabla} \cdot \vec{u} &= 0 \\ (\epsilon_0 + p_0) \frac{\partial \vec{u}}{\partial t} + \vec{\nabla}(\delta p) &= 0. \end{aligned} \quad (8.4)$$

Actually, here the first equation is the energy conservation and the second one is the Newton’s second law.

The small change in pressure  $p$  is related to the small change in energy density  $\epsilon$  by the adiabatic equation:

$$\frac{\delta p}{\delta \epsilon} = \left( \frac{\partial p}{\partial \epsilon} \right)_s \Rightarrow \delta p = c_s^2 \delta \epsilon. \quad (8.5)$$

The standard procedure with the system (8.4) leads to the wave equation both for  $\delta p(x, y, z, t)$  and  $\delta \epsilon(x, y, z, t)$  (see Ref.):

$$\nabla^2(\delta p) - \frac{1}{c_s^2} \frac{\partial^2(\delta p)}{\partial t^2} = 0 \quad (8.6)$$

$$\nabla^2(\delta\epsilon) - \frac{1}{c_s^2} \frac{\partial^2(\delta\epsilon)}{\partial t^2} = 0. \quad (8.7)$$

We focus on the last equation which is a second order partial differential homogeneous equation. In case of a jet propagation which is a source of sound waves, in the rhs of (8.7) there will be some function  $f(x, y, z, t)$  describing the source, and making the equation nonhomogeneous:

$$\nabla^2(\delta\epsilon) - \frac{1}{c_s^2} \frac{\partial^2(\delta\epsilon)}{\partial t^2} = f(x, y, z, t). \quad (8.8)$$

Our goal is to solve the equation (8.8) which is carried out as follows. First we should find the solution of the homogeneous equation (8.7). In turn it can be rewritten in terms of cylindrical-coordinate wave equation such as

$$\begin{aligned} \frac{1}{c_s^2} \frac{\partial^2(\delta\epsilon)}{\partial t^2} = \\ = \frac{\partial^2(\delta\epsilon)}{\partial r_t^2} + \frac{1}{r_t} \frac{\partial(\delta\epsilon)}{\partial r_t} + \frac{1}{r_t^2} \frac{\partial^2(\delta\epsilon)}{\partial \varphi^2} + \frac{\partial^2(\delta\epsilon)}{\partial x^2}, \end{aligned} \quad (8.9)$$

where  $\delta\epsilon \equiv \delta\epsilon(r_t, \varphi, x, t)$ ,  $r_t^2 = y^2 + z^2$ , and the  $\varphi$  is the azimuthal angle. The solution to the cylindrical-coordinate wave equation can be found using the separation of variables:

$$\delta\epsilon(r_t, \varphi, x, t) = R(r_t) \Phi(\varphi) X(x) T(t). \quad (8.10)$$

Solving by this way one gets two final solutions in what follows.

$$\delta\epsilon_{k_t, k, n} = A_{k_t, k, n}^\pm J_n(k_t r_t) e^{\pm i \sqrt{k^2 - k_t^2} x \pm i k c_s t \pm i n \varphi}, \quad (8.11)$$

$$\delta\epsilon_{k_t, k, n} = B_{k_t, k, n}^\pm Y_n(k_t r_t) e^{\pm i \sqrt{k^2 - k_t^2} x \pm i k c_s t \pm i n \varphi}, \quad (8.12)$$

where  $k_t$  and  $k_x = \sqrt{k^2 - k_t^2}$  are the transverse and longitudinal momenta, and  $J_n(k_t r_t)$  and  $Y_n(k_t r_t)$  are the Bessel functions of the first and second kind. The  $A_{k_t, k, n}^\pm$  and  $B_{k_t, k, n}^\pm$  are some constants coming from solutions with the separate variables. The notation in the exponent of (8.11) (or (8.12)) means that there are eight combinations of the sum corresponding to positive and negative values of  $x$ ,  $k$  and  $\varphi$ . At azimuthal symmetry the term  $\frac{1}{r_t^2} \frac{\partial^2(\delta\epsilon)}{\partial \varphi^2}$  from (8.9) is dropped out which means that  $n = 0$  in (8.11) and (8.12). Thus we can rewrite them as

$$\delta\epsilon_{k_t, k} = A_{k_t, k}^\pm J_0(k_t r_t) e^{\pm i (\sqrt{k^2 - k_t^2} x + k c_s t)}, \quad (8.13)$$

$$\delta\epsilon_{k_t, k} = B_{k_t, k}^\pm Y_0(k_t r_t) e^{\pm i (\sqrt{k^2 - k_t^2} x + k c_s t)}, \quad (8.14)$$

and (8.8) as

$$\frac{\partial^2(\delta\epsilon)}{\partial t^2} - c_s^2 \nabla^2(\delta\epsilon) = f(t, x, y, z). \quad (8.15)$$

In this case in the exponent of (8.13) (or (8.14)) there are four combinations of the sum corresponding to positive and negative values of  $x$  and  $k$ .

We solve this last equation using (8.13) and/or (8.14). Suppose we use (8.13). Then the operators in the l.h.s. of (8.15) take the following forms:

$$\frac{\partial^2(\delta\epsilon)}{\partial t^2} = -\omega^2 \left[ A_{k_t, k}^\pm J_0(k_t r_t) e^{\pm i (\sqrt{k^2 - k_t^2} x + \omega t)} \right], \quad (8.16)$$

$$\begin{aligned} -c_s^2 \nabla^2(\delta\epsilon) = \\ = c_s^2 (k_t^2 + k_x^2) \times \\ \times \left[ A_{k_t, k}^\pm J_0(k_t r_t) e^{\pm i (\sqrt{k^2 - k_t^2} x + \omega t)} \right]. \end{aligned} \quad (8.17)$$

By means of these two expressions one can rewrite the solution of (8.15) in the  $\omega$  and  $k$  space, such as

$$[-\omega^2 + c_s^2 (k_t^2 + k_x^2)] \phi_{\omega k} = f_{\omega k} \equiv f(\omega, k). \quad (8.18)$$

The  $f(\omega, k)$  is determined by the Fourier transform of  $f(x, y, z, t)$  which one can choose as a function of the form  $(1/ct_f) \delta(\pm x - ct) \delta(y) \delta(z)$ :

$$\begin{aligned} f(\omega, k) = \\ = \int dt dx dy dz e^{\pm i (\sqrt{k^2 - k_t^2} x + \omega t)} \times \\ \times \frac{1}{ct_f} \delta(\pm x - ct) \delta(y) \delta(z), \end{aligned} \quad (8.19)$$

The  $c$  is the speed of light. From (8.18) the  $\phi_{\omega k}$  is represented as

$$\phi_{\omega k} = \frac{f(\omega, k)}{c_s^2 k^2 - \omega^2}. \quad (8.20)$$

Plugging the result of the integral of (8.19) into this equation we obtain

$$\begin{aligned} (\phi_{\omega k})_+ = \\ = \left( \frac{2\pi}{c^2 t_f} \right) \left( \frac{1}{c_s^2 k^2 - \omega^2} \right) \delta\left(\frac{\omega}{c} - k_x\right), \\ (\phi_{\omega k})_- = \\ = \left( \frac{2\pi}{c^2 t_f} \right) \left( \frac{1}{c_s^2 k^2 - \omega^2} \right) \delta\left(\frac{\omega}{c} - (-k_x)\right). \end{aligned} \quad (8.21)$$

The  $(\phi_{\omega k})_+$  is for positive  $k_x$ , and the  $(\phi_{\omega k})_-$  is for negative  $k_x$ . Carrying out the inverse Fourier transform of  $\phi_{\omega k}$  along with (8.21) we get

$$\begin{aligned} [\phi(t, x, y, z)]_+ = [\delta\epsilon(t, x, y, z)]_+ = \\ = \int \frac{d\omega d^3 k}{(2\pi)^4} e^{\mp i (\omega t - k_x x)} (\phi_{\omega k})_+, \\ [\phi(t, x, y, z)]_- = [\delta\epsilon(t, x, y, z)]_- = \\ = \int \frac{d\omega d^3 k}{(2\pi)^4} e^{\mp i (\omega t - (-k_x) x)} (\phi_{\omega k})_-, \end{aligned} \quad (8.22)$$

which consecutively results in

$$\begin{aligned}
& [\delta\epsilon(t, x, y, z)]_+ = \\
& = \frac{1}{(2\pi)^3 c t_f} \int e^{\mp i(k_x c t - (k_x x + k_y y + k_z z))} \times \\
& \times \frac{dk_x dk_y dk_z}{c_s^2(k_x^2 + k_y^2 + k_z^2) - c^2 k_x^2}, \\
& [\delta\epsilon(t, x, y, z)]_- = \\
& = \frac{1}{(2\pi)^3 c t_f} \int e^{\mp i(-k_x c t + (k_x x + k_y y + k_z z))} \times \\
& \times \frac{dk_x dk_y dk_z}{c_s^2(k_x^2 + k_y^2 + k_z^2) - c^2 k_x^2}, \quad (8.23)
\end{aligned}$$

then

$$\begin{aligned}
\Rightarrow [\delta\epsilon(t, x, y, z)]_+ &= \\
& = \frac{1}{(2\pi)^3 c t_f} \int dk_x e^{\mp i(k_x c t - k_x x)} \times \\
& \times \int dk_t d\varphi \frac{k_t e^{\mp i k_t r_t \cos \varphi}}{c_s^2(k_x^2 + k_t^2) - c^2 k_x^2}, \\
& [\delta\epsilon(t, x, y, z)]_- = \\
& = \frac{1}{(2\pi)^3 c t_f} \int dk_x e^{\mp i(-k_x c t + k_x x)} \times \\
& \times \int dk_t d\varphi \frac{k_t e^{\pm i k_t r_t \cos \varphi}}{c_s^2(k_x^2 + k_t^2) - c^2 k_x^2}, \quad (8.24)
\end{aligned}$$

$$\begin{aligned}
\Rightarrow [\delta\epsilon(t, x, y, z)]_+ &= \\
& = \frac{1}{(2\pi)^2 c t_f} \int dk_x e^{\mp i(k_x c t - k_x x)} \times \\
& \times \int dk_t \frac{(k_t/c_s^2) J_0(k_t r_t)}{k_t^2 + [(c_s^2 - c^2)/c_s^2] k_x^2}, \\
& [\delta\epsilon(t, x, y, z)]_- = \\
& = \frac{1}{(2\pi)^2 c t_f} \int dk_x e^{\mp i(-k_x c t + k_x x)} \times \\
& \times \int dk_t \frac{(k_t/c_s^2) J_0(k_t r_t)}{k_t^2 + [(c_s^2 - c^2)/c_s^2] k_x^2}. \quad (8.25)
\end{aligned}$$

In the integral over  $k_t$  the first order pole is

$$k_t = \pm i \sqrt{\frac{c_s^2 - c^2}{c_s^2}} k_x. \quad (8.26)$$

Hereby, we further have

$$\begin{aligned}
& [\delta\epsilon(t, x, y, z)]_+ = \\
& = \frac{(2\pi i)}{(2\pi)^2 c t_f} \int dk_x e^{\mp i(k_x c t - k_x x)} \times \\
& \times \left[ \frac{(k_t/c_s^2) J_0(k_t r_t)}{2k_t} \right]_{k_t = \pm i \sqrt{\frac{c_s^2 - c^2}{c_s^2}} k_x}, \\
& [\delta\epsilon(t, x, y, z)]_- = \\
& = \frac{(2\pi i)}{(2\pi)^2 c t_f} \int dk_x e^{\mp i(-k_x c t + k_x x)} \times \\
& \times \left[ \frac{(k_t/c_s^2) J_0(k_t r_t)}{2k_t} \right]_{k_t = \pm i \sqrt{\frac{c_s^2 - c^2}{c_s^2}} k_x}, \quad (8.27)
\end{aligned}$$

$$\begin{aligned}
\Rightarrow [\delta\epsilon(t, x, y, z)]_+ &= \\
& = \frac{i}{4\pi c_s^2 c t_f} \int dk_x e^{\mp i(k_x c t - k_x x)} \times \\
& \times J_0\left(\pm i \sqrt{\frac{c_s^2 - c^2}{c_s^2}} r_t k_x\right), \\
& [\delta\epsilon(t, x, y, z)]_- = \\
& = \frac{i}{4\pi c_s^2 c t_f} \int dk_x e^{\mp i(-k_x c t + k_x x)} \times \\
& \times J_0\left(\pm i \sqrt{\frac{c_s^2 - c^2}{c_s^2}} r_t k_x\right). \quad (8.28)
\end{aligned}$$

Ultimately, the integration of two integrals in (8.28) gives the following solutions for the function  $\delta\epsilon(t, x, y, z)$ :

$$\begin{aligned}
& [\delta\epsilon(t, x, y, z)]_+ = \\
& = 0, \\
& = -\frac{1}{2\pi c_s c t_f} \frac{1}{\sqrt{c_s^2(x - ct)^2 + (c^2 - c_s^2)r_t^2}}, \\
& = \frac{1}{2\pi c_s c t_f} \frac{1}{\sqrt{c_s^2(x - ct)^2 + (c^2 - c_s^2)r_t^2}}, \\
& = 0, \quad (8.29)
\end{aligned}$$

and

$$\begin{aligned}
& [\delta\epsilon(t, x, y, z)]_- = \\
& = 0, \\
& = \frac{1}{2\pi c_s c t_f} \frac{1}{\sqrt{c_s^2(x - ct)^2 + (c^2 - c_s^2)r_t^2}}, \\
& = -\frac{1}{2\pi c_s c t_f} \frac{1}{\sqrt{c_s^2(x - ct)^2 + (c^2 - c_s^2)r_t^2}}, \\
& = 0. \quad (8.30)
\end{aligned}$$

Combining the solutions which are in (8.29) and (8.30) we obtain

$$\begin{aligned} [\delta\epsilon(t, x, y, z)]_+ &= [\delta\epsilon(t, x, y, z)]_- = \\ &= \pm \frac{1}{2\pi c_s c t_f} \frac{1}{\sqrt{c_s^2(x - ct)^2 + (c^2 - c_s^2)(y^2 + z^2)}} \cdot \\ &= 0. \end{aligned} \quad (8.31)$$

Generally, the function  $f(t, x, y, z)$  in equation (8.15)

can include some constant  $A$  which has a dimension of  $\text{GeV}/fm$ . Taking also into account this constant we have

$$\begin{aligned} \delta\epsilon(t, x, y, z) &= \\ &= \frac{1}{2\pi c_s c t_f} \frac{A}{\sqrt{c_s^2(x - ct)^2 + (c^2 - c_s^2)(y^2 + z^2)}} \end{aligned} \quad (8.32)$$

One can make this constant  $A$  equal to  $dE/dx$  which is the loss of the jet energy per unit path length.

- 
- [1] E. Shuryak, Phys. Rev. C **80**, 054908 (2009) [Erratum-ibid. C **80**, 069902 (2009)] [arXiv:0903.3734 [nucl-th]].
  - [2] P. Staig and E. Shuryak, [arXiv:1008.3139 [nucl-th]].
  - [3] P. Staig and E. Shuryak, [arXiv:1105.0676 [nucl-th]].
  - [4] J. Casalderrey-Solana, E. V. Shuryak and D. Teaney, J. Phys. Conf. Ser. **27**, 22 (2005) [Nucl. Phys. A **774**, 577 (2006)] [arXiv:hep-ph/0411315].
  - [5] L. M. Satarov, H. Stoecker and I. N. Mishustin, Phys. Lett. B **627**, 64 (2005) [arXiv:hep-ph/0505245].
  - [6] P. M. Chesler and L. G. Yaffe, Phys. Rev. Lett. **99**, 152001 (2007) [arXiv:0706.0368 [hep-th]].
  - [7] S. S. Gubser, A. Nellore, S. S. Pufu and F. D. Rocha, Phys. Rev. Lett. **101**, 131601 (2008) [arXiv:0804.1950 [hep-th]].
  - [8] B. Betz, J. Noronha, G. Torrieri, M. Gyulassy and D. H. Rischke, Phys. Rev. Lett. **105**, 222301 (2010) [arXiv:1005.5461 [nucl-th]].
  - [9] L.D. Landau and E.M. Lifshitz, *Fluid Mechanics*, Vol. **6** (1987).
  - [10] E. V. Shuryak, Phys. Rev. C **76**, 047901 (2007) [arXiv:0706.3531 [nucl-th]].
  - [11] E. V. Shuryak, Phys. Rev. C **66**, 027902 (2002). [nucl-th/0112042].
  - [12] A. Drees, H. Feng, J. Jia, Phys. Rev. C **71**, 034909 (2005). [nucl-th/0310044].
  - [13] J. Liao and E. Shuryak, Phys. Rev. Lett. **102**, 202302 (2009) [arXiv:0810.4116 [nucl-th]].
  - [14] C. Marquet and T. Renk, Phys. Lett. B **685**, 270 (2010) [arXiv:0908.0880 [hep-ph]].
  - [15] F. Dominguez, C. Marquet, A. Mueller, B. Xiao and B. Wu, Nucl. Phys. A **811**, 197 (2008) [arXiv:0803.3234 [hep-ph]].
  - [16] P. M. Chesler, K. Jensen, A. Karch, L. G. Yaffe, Phys. Rev. D **79**, 125015 (2009). [arXiv:0810.1985 [hep-th]]
  - [17] D. Teaney, J. Lauret and E. V. Shuryak, Phys. Rev. Lett. **86**, 4783 (2001) [arXiv:nucl-th/0011058]. "A hydrodynamic description of heavy ion collisions at the SPS and RHIC," [arXiv:nucl-th/0110037].
  - [18] T. Hirano, Acta Phys. Polon. B **36**, 187 (2005) [arXiv:nucl-th/0410017].
  - [19] C. Nonaka and S. A. Bass, Phys. Rev. C **75**, 014902 (2007) [arXiv:nucl-th/0607018].
  - [20] P. Romatschke and U. Romatschke, Phys. Rev. Lett. **99**, 172301 (2007) [arXiv:0706.1522 [nucl-th]].
  - [21] K. Dusling and D. Teaney, Phys. Rev. C **77**, 034905 (2008) [arXiv:0710.5932 [nucl-th]].
  - [22] U. W. Heinz and H. Song, [arXiv:0806.0352 [nucl-th]].
  - [23] R. Andrade, F. Grassi, Y. Hama and W. L. Qian, [arXiv:0912.0703 [nucl-th]].
  - [24] J. Casalderrey-Solana and E. V. Shuryak, [arXiv:hep-ph/0511263].
  - [25] P.F Kolb and U.W. Heinz, Nucl. Phys. A **715**, 653 (2003) [arXiv:nucl-th/0208047].
  - [26] J. Knoll, Phys. Polon. B **40**, 1037 (2009) [arXiv:0902.2373 [nucl-th]]. Nucl. Phys. A **821**, 235 (2009) [arXiv:0803.2343 [nucl-th]].
  - [27] M. Lisa, Braz. J. Phys. **37**, no3a (2007).
  - [28] K. J. Eskola, H. Honkanen, H. Niemi, P. V. Ruuskanen, and S. S. Rasanen, Phys. Rev. C **72**, 044904 (2005).
  - [29] P.F Kolb, Heavy Ion Physics **21**, 243 (2004) [arXiv:nucl-th/0304036].
  - [30] E. Shuryak, [arXiv:1101.4839 [nucl-th]].
  - [31] F. Cooper, G. Frye, Phys. Rev. D **10**, 186 (1974).
  - [32] R. Baier, P. Romatschke, Eur. Phys. J. C **51**, 677 (2007) [arXiv:nucl-th/0610108].
  - [33] M. M. Aggarwal *et al.* [STAR Collaboration], Phys. Rev. C **82**, 024912 (2010) [arXiv:1004.2377 [nucl-ex]].